ACS Photonics

Article

pubs.acs.org/journal/apchd5

Rise of the Charge Transfer Plasmon: Programmable Concatenation of Conductively Linked Gold Nanorod Dimers

Jake Fontana,* Nicholas Charipar, Steven R. Flom, Jawad Naciri, Alberto Piqué, and Banahalli R. Ratna

Naval Research Laboratory, 4555 Overlook Ave SW, Washington, D.C. 20375, United States

Supporting Information

ABSTRACT: The ability to tune the resonant frequency in plasmonic nanostructures is fundamental to developing novel optical properties and ensuing materials. Recent theoretical insights have shown through the conductive concatenation of plasmonic nanoparticles that the effective depolarization factor of the nanostructure, and subsequent charge transfer plasmon (CTP) resonance, can be intricately controlled [Fontana, J.; Ratna, B. R. *Appl. Phys. Lett.* **2014**, *105*, 011107]. However, translating these charge transfer properties from proof-of-principle experiments to high-quality, macroscale quantities for material applications remains challenging. Here, we experimentally demonstrate by using an electrostatic-based molecular assembly approach how to controllably concatenate gold nanorods end-to-end into discrete dimers, preventing unwanted longer structures and forming a capacitively coupled plasmon (CCP) resonance along the long axis of the dimer. Irradiating these suspensions with femtosecond laser pulses at the CCP dimer resonance wavelength selectively welds only the CCP dimers together, bridging the nanorods with gold nanojunctions and producing large, high-quality yields of welded dimers. Macroscale ($\sim 10^{12}$ dimers) absorbance measurements reveal a CTP resonance arising from these welded dimers with absorbance peak magnitudes as large as 0.5 and full-width-at-half-maximum of 274 nm. We show by controlling the aspect ratio of the welded dimers that the CTP absorbance wavelength can differ significantly (~20%) from a single nanorod with a similar aspect ratio, demonstrating the ability to modulate the effective depolarization factor of the dimer structures and resulting CTP resonance. We also carried out three-dimensional finite element simulations showing less than a 5% shift in the CTP absorbance wavelength as a function of the contact point connecting the nanorods and relative orientation, in agreement with our experiments.

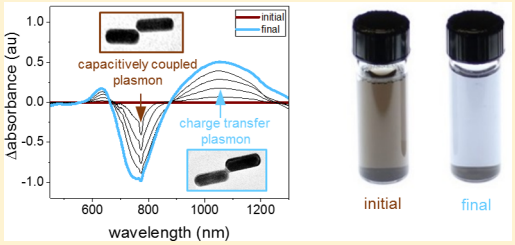

KEYWORDS: *gold, nanorods, plasmonics, charge-transfer plasmon, self-assembly, femtosecond laser*

The optical properties of materials, such as their absorption, transmission, reflection, and refractive index, arise from the interaction of light with matter. Over the past decade, a renaissance has occurred in the understanding of light−matter interactions. Conduction electrons in metallic nanoparticles couple strongly with light, exciting localized surface plasmon resonances, focusing electromagnetic fields below the diffraction limit. This ability to confine light to nanometer-length scales has led to optical metamaterials[1−15] as well as nanoscale lasers[16,17] and antennas.[18−24]

These exquisite optical properties are fundamentally based on resonance and can be described well by a simple harmonic oscillator, or Drude, model.[25] The resonance frequency, $\omega_0 = \sqrt{N}\omega_p$, depends on two parameters: the plasma frequency, ω_p, and the depolarization factor, N. The plasma frequency is material dependent and is proportional to the free electron density. Tuning the plasma frequency has been thoroughly explored using a wide variety of plasmonic materials ranging from aluminum to doped oxides, shifting the resonance from ultraviolet to infrared wavelengths.[26−28] By contrast, the depolarization factor is determined by the shape of the individual plasmonic structures, offering an alternative means to control the resonant frequency.

Conventionally, plasmonic properties originate from the *local* resonances of electrons on the surface of *individual* plasmonic nanoparticles. However, if two gold nanospheres are conductively coupled via a thin metallic bridge, charge is transferred at optical frequencies between each nanoparticle, giving rise to a *nonlocal* CTP resonance with extraordinary tunability.[29,30] Furthermore, if the material of these CTP nanostructures is held constant, changing only the shape and therefore the effective depolarization factor, then the CTP resonance can be drastically modulated. Specifically, if two gold nanorods are conductively coupled end-to-end with a thin gold bridge, the CTP resonance is posited to depend linearly on the nanorod aspect ratio, mimicking a single nanorod much larger in size.[31] The ability for these CTP nanostructures to mimic complex or hard to build nanostructures, tuning the electric and possibly magnetic resonances to prescribed frequencies, may have profound consequences.

A challenging practical limitation to benefit from these properties is producing the intricate nanostructures while simultaneously providing high-throughput for material applications. One approach is to carefully direct the self-assembly of

Received: March 14, 2016
Published: April 27, 2016

DOI: 10.1021/acsphotonics.6b00184
ACS Photonics 2016, 3, 904−911

plasmonic nanoparticles, offering the opportunity for macroscale assembly with nanoscale resolution. A disruptive and elegant strategy to build high-throughput nanostructures using molecular assembly and specialized light was recently demonstrated.[32] Pumpkin-shaped molecules were used to assemble chains of nanospheres and subsequently irradiated with femtosecond laser light. Upon irradiation, the localized "hot-spots" between the nanospheres nonthermally melt, welding the nanospheres together. Recent experiments have been carried out demonstrating that gold nanorods can be welded together into oligomers.[33] The specificity and yield of welded oligomers using this approach was very low with CTP absorbance peaks <0.1 and full-width-at-half-maximum (fwhm) ≫ 500 nm. These oligomer experiments do not demonstrate the controlled concatenation and welding of the nanorods but instead show random agglomeration, which is expected upon exposure to an intense laser pulse. Moreover, the only way to extend the applicability of this laser-based technique is by controlling the configuration (or orientation) by which the nanorods assemble. Consequently, there remains a significant need for alternative approaches to efficiently produce large, high-quality yields of welded nanorod dimers.

Here, we demonstrate an approach to controllably weld gold nanorods end-to-end, forming dimers in macroscale quantities while controlling the nanometer-sized junctions linking the nanorods via molecular assembly and femtosecond light. We show using electrostatic-based molecular assembly the discrete selection of CCP end-to-end dimer assemblies, preventing larger structures. We establish that large, high-quality yields of welded dimers (~10^{12} dimers per hour) can be produced by illuminating these dimer suspensions at their CCP resonance wavelength with femtosecond light. From in situ absorbance measurements, we observed an isosbestic point transitioning the single nanorods to CCP dimers, indicative of direct population conversion. A second isosbestic point, and population conversion, is measured transitioning the CCP dimer to welded dimers upon femtosecond irradiation, giving rise to a CTP absorbance peak with magnitudes as large as 0.5 and fwhm = 274 nm. Transmission electron microscopy (TEM) imagery confirms these dimers are welded end-to-end with gold nanojunctions connecting the nanorods. We find by controlling the aspect ratio of the welded dimers that the CTP absorbance wavelength differs significantly (~20%) from that of a single nanorod with a similar aspect ratio, demonstrating the ability to modulate the effective depolarization factor of the dimer structure and thereby control the CTP resonance wavelength. We observe little dependence on the nanojunction geometry and resulting CTP resonance wavelength as a function of laser fluence ranging from 20 μJ/cm^2 per pulse to 600 μJ/cm^2 per pulse. Three-dimensional finite element simulations were carried out to support the experimental measurements and gain insights into the optical responses of the welded dimers for different spatial and orientational distributions. We find a small (<5%) shift in the CTP absorbance wavelength by varying the contact point connecting the nanorods and the relative orientation. These numerical results agree well with TEM imagery of the welded dimer morphologies and the relatively large experimentally measured CTP quality factors determined from spectroscopy.

RESULTS AND DISCUSSION

Experiments were carried out using aqueous suspensions of poly(acrylic acid) (PAA)-coated gold nanorods mixed into a cuvette containing a disodium chromoglycate (DSCG) solution, Figure 1(a).[34] The negatively charged PAA coats

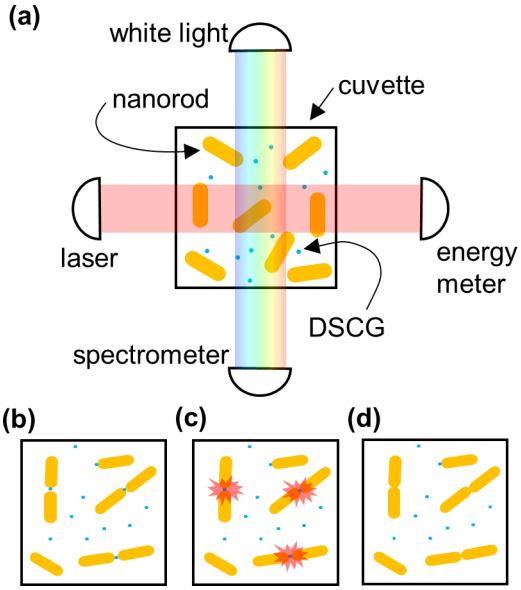

Figure 1. (a) Schematic of the experimental setup (top view). (b) Molecular assisted end-to-end assembly of nanorod dimers. (c) Femtosecond irradiation. (d) Welded nanorod dimers and partially reacted single nanorods.

only the cylindrical portion of the nanorods initially stabilized with a positively charged surfactant, cetyltrimethylammonium bromide (CTAB), leaving the hemispherical ends bare. Upon mixing of the DSCG molecules with the suspension, they are electrostatically repelled from the cylindrical portion of the nanorods coated with PAA and begin to attach at the nanorod ends. Slowly, over the course of hours, the nanorods are incubated, forming concatenated nanorod dimers via the $\pi-\pi$ stacking of the DSCG molecules, Figure 1b. Once the reaction has yielded the maximum concatenated dimer population, for incubation times between 2 and 3 h (see Supporting Information, Figure 1s), the suspension is irradiated at the concatenated dimer resonant wavelength with femtosecond (fs) laser light, typically at ~150 μJ/cm^2 per pulse for 30 min (see Methods section), welding the dimers together, Figure 1c and 1d. The suspension is probed in situ with an unpolarized white light source and spectrophotometer oriented orthogonally to the laser beam as depicted in Figure 1a.[32]

The experimental evolution of the absorbance spectrum for the DSCG molecular assisted end-to-end concatenation of gold nanorod dimers with length (L) to diameter (D) aspect ratios (L/D) of 2.75 (55/20 nm) is shown in Figure 2a. The nanorods are isotropic in the suspension. Two absorbance peaks are initially measured (red curve) corresponding to the transverse surface plasmon (TSP) resonance along the short axis of the nanorod at 515 nm and longitudinal surface plasmon (LSP) resonance along the long axis of the nanorod at 694 nm. After mixing the suspension with the DSCG solution, a sharp isosbestic point forms at 750 nm, signifying two distinct nanorod populations as the concatenated dimer assemblies are created. A third absorbance peak begins to emerge at 775 nm corresponding to the CCP resonance from the capacitively coupled end-to-end nanorod dimers, Figure 2a (brown curve). TEM images confirm the suspension is composed of single and

DOI: 10.1021/acsphotonics.6b00184
ACS Photonics 2016, 3, 904−911

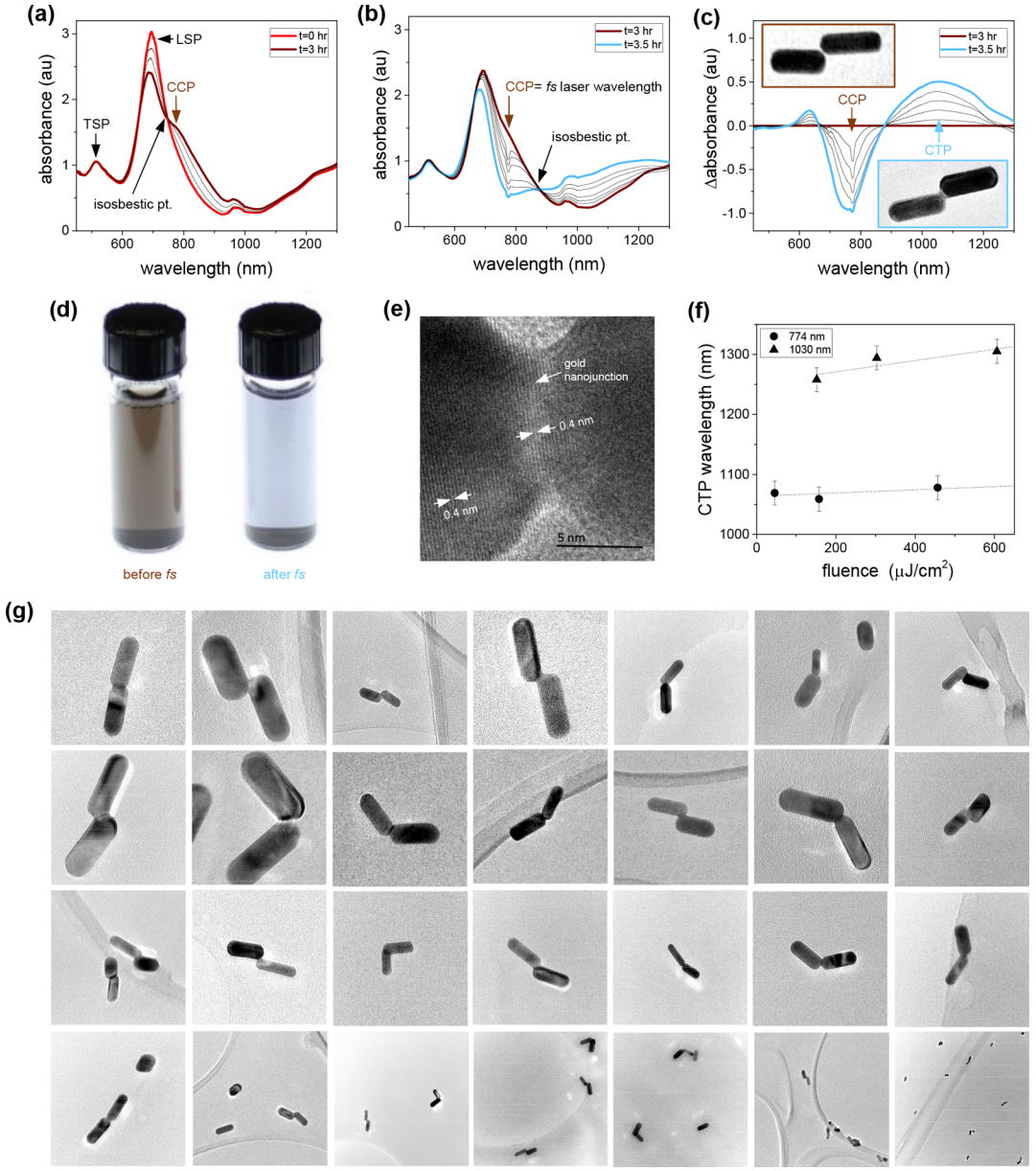

Figure 2. (a) Experimental absorbance spectrum evolution for the DSCG molecular-assisted end-to-end concatenation of gold nanorod dimers (55/20 nm) for incubation times from 0 (red curve) to 3 (brown curve) hours. (b) Experimental absorbance spectrum evolution of the concatenated nanorod dimer suspension (incubation time = 3 h) upon femtosecond irradiation at CCP = 775 nm (laser wavelength = 774 nm, pulse energy = 20 μJ, repetition rate = 1 kHz, pulse width = 275 fs, irradiated suspension volume $\approx$ 100 mm^3) from 0 min (brown curve) to 30 min (blue curve). (c) Differential absorbance from (b). Representative TEM images of the nanorod dimers before femtosecond laser irradiation (upper left inset) and after irradiation (lower right inset). (d) Images of the nanorod suspension before (left, brown) and after (right, blue) femtosecond exposure and welded dimer formation. (e) TEM image of a magnified nanojunction connecting the nanorods. (f) CTP absorbance peak wavelength of welded dimers (LSP = 675 nm, CCP = 775 nm) versus femtosecond laser pulse energy per area irradiated at 774 and 1030 nm. (g) Representative TEM images of welded end-to-end gold nanorod dimers. The average nanorod size is D = 20 nm, L = 55 nm.

end-to-end dimer assemblies for incubation times less than 3 h with a typical small lateral shift from the triangular facets of the nanorod ends, consistent with the literature.[34] If the reaction is allowed to continue for incubation times up to 24 h, longer linear assemblies can be created. The upper-left insert in Figure 2c shows a representative TEM image of a concatenated dimer before irradiation. The age of the gold nanorods greatly influences the rate the nanorods concatenate. We found that the nanorods are the most reactive one week after synthesis and slowly dampen over the course of weeks. Experiments were typically carried out with nanorods less than one month old.

The suspension in the cuvette at an incubation time of 3 h (Figure 2b, brown curve) is then irradiated with unfocused femtosecond laser light for 30 min (wavelength = 774 nm, pulse energy = 20 μJ, repetition rate = 1 kHz, pulse width = 275 fs, irradiated suspension volume $\approx$ 100 mm^3) at the dimer (CCP = 775 nm) resonance wavelength, selectively welding only the concatenated dimers together. The suspension can continue to incubate until additional dimers are formed, which are then "seen" by the laser light and welded together. Using this approach in principle enables all the single nanorods to be controllably processed into welded dimers. Figure 2b is the

DOI: 10.1021/acsphotonics.6b00184
ACS Photonics 2016, 3, 904−911

experimental evolution of the absorbance spectrum as the suspension is irradiated with femtosecond laser light at the CCP wavelength. The sharp dip at 774 nm is due to scattering and instantaneously disappears if the laser light is blocked. As the suspension is irradiated, the absorbance at the CCP wavelength begins to decrease, and a second isosbestic point forms at 875 nm, visibly signifying the direct conversion of CCP to a new population (Figure 2b, blue curve). At any point during the welding process, if the suspension was mixed with a pipet, the absorbance remained constant, demonstrating processing of the entire suspension.

From the differential absorbance, Figure 2c, a new absorbance peak clearly emerges at 1050 nm (blue curve), corresponding to the CTP resonance along the entire long axis of the welded dimer. The insets in Figure 2c are representative TEM images of the dimers before irradiation (upper left) and after irradiation (bottom right). The magnitude of the CTP absorbance peak is large with an absorbance on the order of 0.5, demonstrating an efficient yield of welded dimers.[32,33] The fwhm from the new CTP absorbance peak is also large and clearly definable, $fwhm_{CTP}$ = 274 nm, relative to the LSP absorbance peak from the suspension before assembly, $fwhm_{LSP}$ = 113 nm.[32,33] A second smaller absorbance peak also emerges at 635 nm and is attributed to the bonding dipolar plasmon (BDP) mode of the individual nanorods in the welded dimers, providing further evidence that the nanorods are conductively coupled.[29] We found (as the nanorods age) their reactivity and subsequent dimer yields decrease with time, although the evolution of their spectra upon irradiation remained constant, for the dozens of experiments carried out here.

Figure 2d shows a 2 mL suspension of dimers before (left) and after fs irradiation (right) for 30 min (laser wavelength = 774 nm, pulse energy = 20 μJ, repetition rate = 1 kHz, pulse width = 275 fs, irradiated suspension volume $\approx$ 100 mm^3) demonstrating the approach is capable of high-throughput (~ml/h). Increasing the incubation time and decreasing the rate that the dimers are assembled, relative to previous work,[33] from several minutes using a covalent-mediated molecular assembly to several hours using electrostatic assembly, is critical to enable temporal and spatial control over the dimer assembly (see Figure 2s).

The TEM image in Figure 2e is the connected nanojunction between the nanorods, where a periodic lattice can clearly be observed. The Fourier transforms of the nanojunction image in Figure 2e for the nanorod and nanojunction regimes both result in a lattice constant of 0.4 $\pm$ 5% nm, corresponding to the lattice constant of gold.[33]

Representative TEM images of the welded dimers are shown in Figure 2g. The nanorod ensembles predominately consist of individual nanorods and end-to-end welded dimers. Flocculates of nanorods were, although rare, observed during TEM analysis and are the result of evaporative effects and not from welding. A significant advantage of our approach is established by the absence of higher order welded nanostructures in our images over the course of dozens of experiments. These observations are in strong agreement with our spectroscopy measurements showing sharp isosbestic points and high quality resonances, which can only be explained by the direct conversion of individual nanorods to end-to-end welded nanorod dimers.

The fluence from the femtosecond laser was found to be a key parameter to create the welded dimers in agreement with other reports.[32,33] We begin to see evidence of nanorod welding, through spectroscopy and TEM measurements, at approximately 20 $\mu J/cm^2$ per pulse at 774 nm for irradiation times of 60 min, although the rate of CCP to CTP dimers conversion is poor with absorbance changes of less than 0.1. If the fluence is increased to 45 $\mu J/cm^2$ per pulse at 774 nm for 30 min, the rate of CCP to CTP dimers significantly increases, defining a fluence threshold, Figure 2f. Surprisingly, the energy of the pulse has little effect on the geometry of the welded nanojunctions and subsequent CTP absorbance peak. These observations suggest that the welding of the dimers is due to an ignition of a plasma in the nanojunction between the nanorods where the instantaneously excited electrons from the femtosecond pulse are unable to transfer heat to the lattice, causing it to locally weaken and enabling the gold atoms to flow into the nanojunction. The CTP absorbance peak does appear to slightly red shift from 1250 to 1300 nm as a function of fluence at 1030 nm but is below the uncertainty of our measurements; therefore, we are uncomfortable speculating on a possible mechanism to explain this perceived increase.

The rate of CCP to CTP dimers increases as the fluence of the femtosecond laser is increased from 45 to 450 $\mu J/cm^2$ per pulse at 774 nm for 30 min. We found that, if the suspension in Figure 2 is irradiated far from and on the low energy side of the CCP resonance wavelength (775 nm) at 1030 nm or on the high energy side at TSP = 515 nm, welding can still occur with a new CTP absorbance peak emerging at 1300 nm for the 1030 nm irradiation and 877 nm for the 515 nm irradiation. The yield and specificity of these welded nanostructures is poor, producing haphazard nanorod aggregates (see Figures 3s and 4s) as well as increasing the fluence threshold by nearly 3-fold before welding is observed (150 $\mu J/cm^2$ per pulse at 1030 nm for 30 min). It is unclear if the laser at this wavelength induces aggregation or if there is a low percentage of random flocculates in the suspension with resonances that coincide with the laser wavelength. These results demonstrate that irradiating the suspension near the dimer CCP resonance wavelength dramatically improves the yield and quality of the welded dimers.

To understand the relationship between the aspect ratio of the individual nanorods and the CTP wavelength of the welded dimers, two additional nanorod populations were experimentally studied with aspect ratios of 2 (50/25 nm, LSP = 600 nm) and 4 (100/25 nm, LSP = 950 nm). For the 50/25 nm suspensions, after an incubation time of 3 h, the CCP dimer wavelength emerged at 690 nm (see Figures 5s and 6s). The maximum fluence output from the laser at 690 nm was 8 $\mu J/cm^2$ per pulse, which is below the fluence threshold required for welding. For verifying that the dimers could not be welded, the suspension was probed at this fluence for 30 min with no measured change in the absorbance. To initiate the welding process, a lens (focal length = 400 mm) was placed 300 mm in front of the cuvette, such that the beam focused 100 mm behind the cuvette, maintaining a quasi-parallel beam through the cuvette. The introduction of the lens increased the fluence to just above the absolute minimum fluence threshold to 24 $\mu J/cm^2$ per pulse at 690 nm while decreasing the irradiated volume inside the cuvette by over half to ~40 mm^3. Figure 3a shows the spectral evolution of the differential absorbance for the 50/25 nm suspension irradiated with femtosecond laser light at the CCP wavelength (690 nm) for 30 min. A scattering dip at 690 nm was not observed in contrast to the 774 nm case, due in part to the small laser fluence. As the suspension was irradiated, the absorbance at the CCP wavelength begins to decrease, a second isosbestic point forms at 738 nm, and the CTP

DOI: 10.1021/acsphotonics.6b00184
ACS Photonics 2016, 3, 904−911

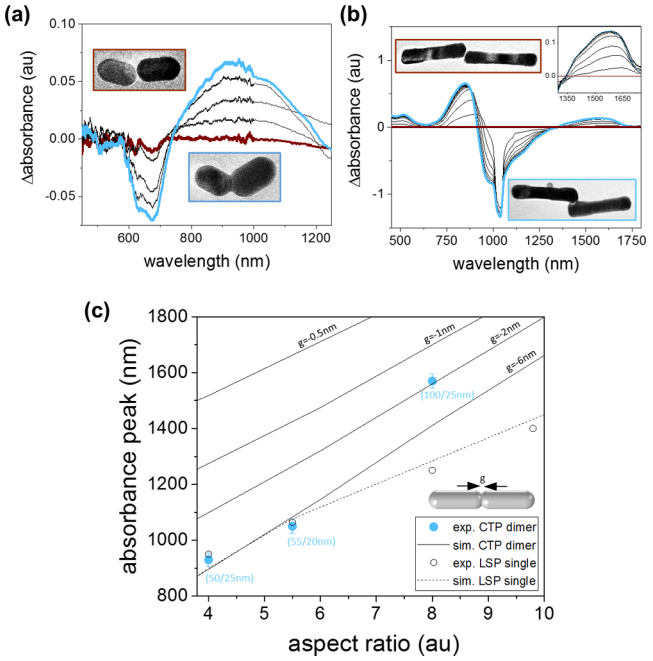

Figure 3. Differential absorbance spectra from suspensions (a) 50/25 nm (LSP = 600 nm, CCP = 690 nm) and (b) 100/25 nm (LSP = 950 nm, CCP = 1200 nm) irradiated for 30 min at 690 nm (pulse energy = 1.0 μJ, repetition rate = 1 kHz, pulse width ≈ 150 fs, beam area ≈ 4.1 mm^2) and 1030 nm (pulse energy = 20 μJ, repetition rate = 1 kHz, pulse width = 280 fs, beam area = 19.81 mm^2), respectively. Representative TEM images of the nanorod dimers are shown before (inset in the upper left) and after (inset in the lower right) femtosecond laser irradiation. The inset in the upper-right of (b) is the magnified CTP absorbance peak regime. (c) Absorbance peak wavelength as a function of the dimer aspect ratio. The solid blue dots are the experimental CTP absorbance peaks from the welded dimer nanostructures (50/25, 55/20, and 100/25 nm). The solid black lines are the simulated CTP absorbance peaks as a function of end-to-end overlap gap from −6 to −0.5 nm. The open black circles are the experimental LSP absorbance peaks from single gold nanorods with equivalent aspect ratios to the welded dimers, and the dashed black line is the simulated LSP absorbance peaks from single gold nanorods.

absorbance peak emerges at 925 nm (Figure 3a, blue curve). The inset in the upper left of Figure 3a is a representative TEM image of the dimer before irradiation and the inset in the bottom right is after irradiation. Although clearly measurable and repeatable both spectrally and using TEM, the relatively small magnitude of the CTP absorbance peak at 925 nm is a consequence of the small laser fluence.

Figure 3b is the spectral evolution of the differential absorbance for the 100/25 nm suspension, irradiated at 600 μJ/cm^2 per pulse at 1030 nm for 30 min, slightly off the CCP resonance (1200 nm) and on the high energy side of the peak (see Figures 7s and 8s), although still overlapping with the LSP absorbance peak. A dip in the absorbance spectra is again observed at 1030 nm from the scattered laser light. As the suspension is irradiated, the absorbance at 1030 nm, near the CCP wavelength, begins to decrease, an isosbestic point plainly forms at 1300 nm, and the CTP absorbance peak emerges at 1570 nm (Figure 3b, blue curve). The magnitude of the CTP peak is relatively small, and in contrast to Figure 2c, the spectra of single nanorods also begin to emerge with the observation of TSP (517 nm) and LSP (848 nm) peaks. This may be due to the laser wavelength not exactly matching the CCP absorbance wavelength, thus producing a lower yield of welded dimers and possibly disassociating or destroying the DSCG molecules due to the large laser fluence breaking apart the CCP dimers, leading to a percentage of the population becoming single nanorods. The insets in Figure 3b are representative TEM images of the dimer before (upper left) and after (bottom right) irradiation. The inset in the upper right of Figure 3b is the magnified CTP absorbance peak regime.

Simulations were carried out to understand the evolution of the CTP absorbance wavelength as the cross-sectional area of the welded nanojunction is decreased and as a function of the dimer aspect ratio, $2 \times (L/D)$, Figure 3c (solid black lines). For varying the cross-sectional area of the nanojunction, the nanorods, oriented end-to-end, were overlapped with negative gaps ranging from gap = −6 to −0.5 nm. The simulated (dashed black line) and experimental (open black circles) LSP absorbance peaks from single gold nanorods, with equivalent aspect ratios to the welded dimers, are also shown in Figure 3c for comparison. As expected, the LSP absorbance peak wavelength for a single nanorod depends linearly on the nanorod aspect ratio $\lambda_{LSP} = \sqrt{(\lambda_p^2/N_{\|})} \propto L/D$, where λ_p is the plasma wavelength of gold, and $N_{\|} = (1 - e^2/2e^3)(\ln((1 + e)/(1 - e)) - 2e)$ is the depolarization factor along the long axis of the nanorod with $e = \sqrt{1 - (D/L)^2}$.[25,35] There is a change in the slope of the LSP wavelength for the single nanorods at an aspect ratio of approximately 5.5; this change is also observed in the experimental data (open black circles), validating the simulation data (dashed black line). We also find that the CTP absorbance peak from the simulated dimers depends linearly on the aspect ratio.

Comparing the experimental CTP absorbance peaks as a function of dimer aspect ratio (blue dots) to the simulation results (solid black lines) in Figure 3c, we find for aspect ratios of 4 and 5.5 (individual nanorods 50/25 and 55/20 nm) that the experimental absorbance peaks from the welded dimers agree well with an overlap gap of −6 nm. We find this is also equivalent to a single nanorod with an equivalent aspect ratio as the dimer, i.e., CTP = LSP. These results suggest that the gold nanojunction is sufficiently conductive not to impede the flow of electrons between the small aspect ratio nanorods, enabling these welded dimer structures to behave as a single nanorod. Generalizing this approach, high aspect ratio nanorods of arbitrary length may be assembled from smaller ones by repeating the concatenation and irradiation cycle, building dimers, double dimers, or n dimers, where n is the number of nanorods in the linear nanostructure, possibly providing an approach to alleviate the long-standing issues of creating high aspect ratio plasmonic nanorods.

Remarkably, examining the case of the larger aspect ratio welded dimers (100/25 nm) in Figure 3c, we find a ∼20% deviation in the absorbance peak wavelength to that of a single nanorod (aspect ratio = 8). The welded dimer (100/25 nm) CTP absorbance peak wavelength agrees well with the −2 nm overlap simulations. The material of the welded dimers is constant ($\omega_p^{Au} = 2.18 \times 10^{15}$ s^{-1}); therefore, the change in resonance and the CTP absorbance peak wavelength must come from the shape (N) of the dimers,[31] demonstrating the ability to tune the effective depolarization factor of the dimer and subsequent macroscale CTP absorbance.

To develop an understanding of the changes in the optical response by varying the spatial and orientational distributions of the simulated dimers, further simulations were undertaken,

DOI: 10.1021/acsphotonics.6b00184
ACS Photonics 2016, 3, 904−911

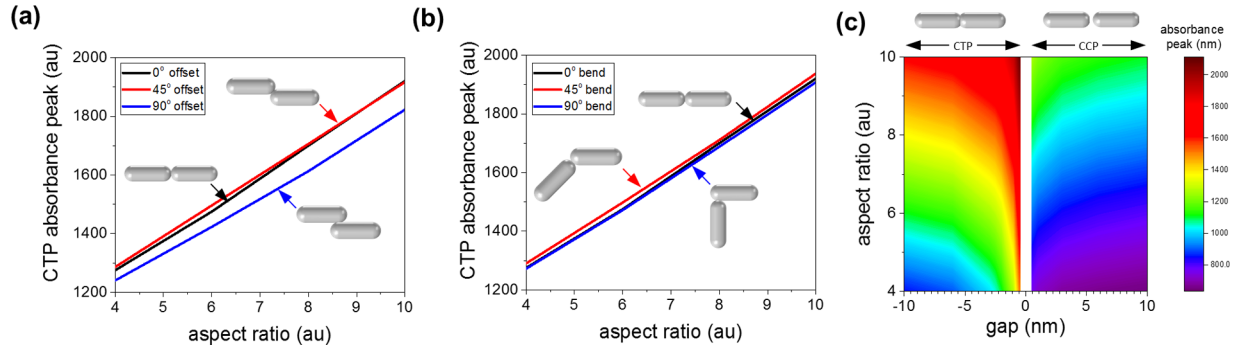

Figure 4. (a) The CTP absorbance peak wavelength for a −1 nm gap overlap and contact point offsets connecting the nanorods at 0°, 45°, and 90° as a function of the dimer aspect ratio. (b) The CTP absorbance peak wavelength for a −1 nm overlap gap for relative dimer orientations of 0°, 45°, and 90° as a function of the dimer aspect ratio. (c) The evolution of the CTP and CCP absorbance peak wavelengths for the dimer aspect ratio as a function of the gap.

Figure 4. The dimers were probed with light polarized along the long axis of the dimer. The position of the welded nanojunction was offset by 0°, 45°, and 90° as a function of the dimer aspect ratio for a constant −1 nm gap overlap with both nanorods remaining colinear, as depicted in Figure 4a. We find less than a 5% difference in the CTP absorbance peak wavelength by varying the offset of the welded nanojunction from 0 to 90°. The 90° offset case is more blue-shifted due to the slightly larger overlapping cross-sectional area relative to the 0° and 45° cases. In Figure 4b, the relative orientation of one of the nanorods composing the welded dimer was rotated by 0°, 45°, and 90° and studied as a function of the dimer aspect ratio for a constant −1 nm gap. We find only approximately a 2% difference in the CTP absorbance peak wavelength by changing the relative orientations of the nanorods from 0 to 90° with respect to one another and by rotating the probe polarization by 90°. These numerical results agree well with the relatively large quality factors from the experimentally measured CTP resonances, implying the distribution of offsets and relative orientations has surprisingly little effect on the CTP resonance wavelength. These results are unexpected and will be further investigated in future work.

Figure 4c shows the evolution of the CTP and CCP absorbance peak wavelengths for the welded and unwelded dimers as a function of dimer aspect ratio and gap. For the CTP case, as the overlap gap decreases from −10 to −0.5 nm, the cross-sectional area of the nanojunction is reduced, leading to the CTP absorbance peak wavelength red-shifting by approximately a factor of 2 for the parameter space probed. As the dimer aspect ratio increases, the CTP absorbance peak wavelength also red-shifts. As expected for the CCP case, as the gap decreases from 10 to 0.5 nm and as the dimer aspect ratio increases from 4 to 10, the CCP absorbance peak wavelength red-shifts, although significantly less than that of the CTP case.

CONCLUSIONS

In summary, we developed an experimental approach using molecular assembly and femtosecond light to controllably weld gold nanorods end-to-end, forming dimers in macroscale quantities. We showed how electrostatic-based molecular assembly enables the discrete selection of CCP end-to-end dimers, preventing larger structures, in contrast to covalent bonding approaches. We demonstrated by illuminating these dimer suspensions at their CCP resonance wavelength with femtosecond laser pulses that large, high-quality yields of welded dimers can be produced (~10^{12} dimers per hour). We measured the evolution of the absorbance spectra from these suspensions and observed an isosbestic point transitioning the single nanorods to CCP dimers. Upon femtosecond irradiation, a second isosbestic point was measured transitioning the CCP dimer to welded dimers and giving rise to a CTP absorbance peak with magnitude as large as 0.5 and fwhm = 274 nm. TEM imagery confirmed these dimers are welded end-to-end with gold nanojunctions connecting the nanorods. We found by controlling the aspect ratio of the welded dimers that the CTP absorbance wavelength differs significantly (~20%) from that of a single nanorod with a similar aspect ratio, demonstrating the ability to modulate the effective depolarization of the dimer structure, because the entire structure is composed of gold, and thus control the CTP resonance wavelength. We found almost no dependence on the nanojunction geometry and subsequent CTP resonance wavelength as a function of laser fluence ranging from 20 to 600 $\mu J/cm^2$ per pulse. Three-dimensional finite element simulations were carried out to understand the optical responses of the welded dimers for different spatial and orientational distributions. We found less than a 5% shift in the CTP absorbance wavelength by varying the contact point connecting the nanorods and the relative orientation, which is in agreement with experimental results.

METHODS

Synthesis. Gold nanorods were synthesized using a seed-mediated method.[36,37] The synthesis reduces $HAuCl_4$ in an aqueous solvent with $NaBH_4$, forming small nanospheres that act as nucleation seeds when added to a growth solution containing gold ions and CTAB. The lattice of the seed has a nonuniform affinity for CTAB, breaking the spherical symmetry and allowing the excess gold ions to precipitate onto the surface of the Au seed at different rates, leading to the formation of nanorods. Gold nanorods were also commercially acquired from Nanopartz, Inc.

Concatenation. Gold nanorods were concatenated into end-to-end dimers using a molecularly assisted self-assembly approach.[34] A cuvette (Starna, 1 cm path length, rectangular, quartz, four optically polished sides) was initially cleaned with Aqua Regia (Nitirc acid: HCL, 1:3), rinsed with deionized (DI) water (18.2 MΩ), cleaned with Piranha solution (sulfuric acid:H_2O_2 (30%), 3:1), once again washed with DI water, and then dried with nitrogen gas. Gold nanorods (0.5 mL, ~0.2 nM) initially stabilized with a positively charged surfactant, CTAB, were coated with PAA (100 μL of 1% PAA, mol wt 250,000), making the nanorods negatively charged after the

DOI: 10.1021/acsphotonics.6b00184
ACS Photonics 2016, 3, 904−911

PAA was adsorbed to the CTAB layer. The PAA solution was slowly added, dropwise, over approximately 1 min while concurrently shaking the suspension. The suspension was then allowed to sit for 15 min. A DSCG solution (0.5 mL, 0.2 M) was added to the PAA-coated nanorod suspension, initiating the end-to-end self-assembly (see Figures 1s, 5s, and 7s).

Lasers. The suspensions were typically incubated between 2 and 3 h, concatenating the dimers, and then irradiated for 30 min, unless otherwise specified. The femtosecond laser pulses at 774 nm were generated from a Clark MXR Chirped Pulse Amplifier CPA 2001 (pulse energy = 1−60 μJ, repetition rate = 1 kHz, pulse width = 275 fs, beam area = 12.74 mm^2) and used to pump a noncollinear optical parametric amplifier (Clark MXR, NOPA) to generate the 690 nm wavelength (pulse energy = 1.0 μJ, repetition rate = 1 kHz, pulse width ≈ 150 fs, beam area ≈ 4.1 mm^2). The 1030 and 515 nm (pulse energy = 1−120 μJ, repetition rate = 1 kHz, pulse width = 280 fs, beam area = 19.81 mm^2) were generated from an amplified Yb:KGW femtosecond laser (Pharos, Light Conversion, Vilnius, Lithuania). The collimated beam probed the sealed (1 cm path length) quartz cuvette containing the concatenated nanorod dimers and was directed into an energy meter (Ophir, PE9-SH head with a Nova II controller), Figure 1a.

Characterization. The welding process was monitored in situ orthogonal to the laser light. An unpolarized white light source (DH-2000) was used to probe the suspension, and the light was collected with a bifurcated optical fiber (OceanOptics QBIF50-VIS-NIR) coupled to spectrophotometers (USB4000 and NIRQuest). The spectra from the two spectrometers were typically spliced together at 1 μm. Transmission electron microscopy (TEM) images were obtained using a JEOL JEM-2200FS field emission electron microscope with 200 kV accelerating voltage. TEM samples were prepared by placing an ∼10 μL drop of the sample suspension onto a carbon-coated copper grid, wicked off with lens paper, and allowed to dry overnight.

Simulations. Numerical simulations were carried out to support experimental results using three-dimensional finite element simulations (COMSOL Multiphysics 5.2). The gold nanorods were modeled as spherocylinders surrounded by water. Using the port geometry, periodic boundary conditions were placed on the entire structure. The refractive indices of gold and water were interpolated from the literature.[38] The gold nanorods were probed with light parallel to the long axis of the nanorods. The S_{21} element from the scattering matrix was retrieved from the simulations and used to calculate the absorbance equal to $-\log(|S_{21}|^2)$.

■ ASSOCIATED CONTENT

Supporting Information

The Supporting Information is available free of charge on the ACS Publications website at DOI: 10.1021/acsphotonics.6b00184.

Additional nanorod/DSCG reactions and welding experiments (PDF)

■ AUTHOR INFORMATION

Corresponding Author

*E-mail: jake.fontana@nrl.navy.mil.

Notes

The authors declare no competing financial interest.

■ REFERENCES

(1) Pendry, J. B. Negative refraction makes a perfect lens. *Phys. Rev. Lett.* **2000**, *85*, 3966−3969.
(2) Shelby, R. A.; Smith, D. R.; Schultz, S. Experimental verification of a negative index of refraction. *Science* **2001**, *292*, 77−79.
(3) Xiao, S. M.; Chettiar, U. K.; Kildishev, A. V.; Drachev, V. P.; Shalaev, V. M. Yellow-light negative-index metamaterials. *Opt. Lett.* **2009**, *34*, 3478−3480.
(4) Drachev, V. P.; Cai, W.; Chettiar, U.; Yuan, H. K.; Sarychev, A. K.; Kildishev, A. V.; Klimeck, G.; Shalaev, V. M. Experimental verification of an optical negative-index material. *Laser Phys. Lett.* **2006**, *3*, 49−55.
(5) Valentine, J.; Zhang, S.; Zentgraf, T.; Ulin-Avila, E.; Genov, D. A.; Bartal, G.; Zhang, X. Three-dimensional optical metamaterial with a negative refractive index. *Nature* **2008**, *455*, 376−9.
(6) Alaeian, H.; Dionne, J. A. Plasmon nanoparticle superlattices as optical-frequency magnetic metamaterials. *Opt. Express* **2012**, *20*, 15781−15796.
(7) Alù, A.; Silveirinha, M. G.; Salandrino, A.; Engheta, N. Epsilon-near-zero metamaterials and electromagnetic sources: Tailoring the radiation phase pattern. *Phys. Rev. B: Condens. Matter Mater. Phys.* **2007**, *75*, 155410.
(8) Smolyaninov, I. I. Transformational optics of plasmonic metamaterials. *New J. Phys.* **2008**, *10*, 115033.
(9) Vignolini, S.; Yufa, N. A.; Cunha, P. S.; Guldin, S.; Rushkin, I.; Stefik, M.; Hur, K.; Wiesner, U.; Baumberg, J. J.; Steiner, U. A 3D Optical Metamaterial Made by Self-Assembly. *Adv. Mater.* **2012**, *24*, OP23−OP27.
(10) Fontana, J.; Ratna, B. R. Toward high throughput optical metamaterial assemblies. *Appl. Opt.* **2015**, *54*, F61−F69.
(11) Chanda, D.; Shigeta, K.; Gupta, S.; Cain, T.; Carlson, A.; Mihi, A.; Baca, A. J.; Bogart, G. R.; Braun, P.; Rogers, J. A. Large-area flexible 3D optical negative index metamaterial formed by nanotransfer printing. *Nat. Nanotechnol.* **2011**, *6*, 402−407.
(12) Dolling, G.; Enkrich, C.; Wegener, M.; Zhou, J. F.; Soukoulis, C. M. Cut-wire pairs and plate pairs as magnetic atoms for optical metamaterials. *Opt. Lett.* **2005**, *30*, 3198−3200.
(13) Veselago, G.; Narimanov, E. E. The left hand of brightness: past, present and future of negative index materials. *Nat. Mater.* **2006**, *5*, 759−762.
(14) Zhang, X.; Liu, Z. W. Superlenses to overcome the diffraction limit. *Nat. Mater.* **2008**, *7*, 435.
(15) Valentine, J.; Li, J. S.; Zentgraf, T.; Bartal, G.; Zhang, X. An optical cloak made of dielectrics. *Nat. Mater.* **2009**, *8*, 568−571.
(16) Bergman, D. J.; Stockman, M. I. Surface Plasmon Amplification by Stimulated Emission of Radiation: Quantum Generation of Coherent Surface Plasmons in Nanosystems. *Phys. Rev. Lett.* **2003**, *90*, 027402.
(17) Noginov, M. A.; Zhu, G.; Belgrave, A. M.; Bakker, R.; Shalaev, V. M.; Narimanov, E. E.; Stout, S.; Herz, E.; Suteewong, T.; Wiesner, U. Demonstration of a spaser-based nanolaser. *Nature* **2009**, *460*, 1110−1112.
(18) Schnell, M.; Garcia-Etxarri, A.; Huber, A. J.; Crozier, K.; Aizpurua, J.; Hillenbrand, R. Controlling the near-field oscillations of loaded plasmonic nanoantennas. *Nat. Photonics* **2009**, *3*, 287−291.
(19) Alber, I.; Sigle, W.; Demming-Janssen, F.; Neumann, R.; Trautmann, C.; van Aken, P. A.; Toimil-Molares, M. E. Multipole Surface Plasmon Resonances in Conductively Coupled Metal Nanowire Dimers. *ACS Nano* **2012**, *6*, 9711−9717.
(20) Aizpurua, J.; Bryant, G. W.; Richter, L. J.; de Abajo, F. J. G.; Kelley, B. K.; Mallouk, T. Optical properties of coupled metallic nanorods for field-enhanced spectroscopy. *Phys. Rev. B: Condens. Matter Mater. Phys.* **2005**, *71*, 235420-1.
(21) Giannini, V.; Fernandez-Dominguez, A. I.; Heck, S. C.; Maier, S. A. Plasmonic nanoantennas: fundamentals and their use in controlling the radiative properties of nanoemitters. *Chem. Rev.* **2011**, *111*, 3888−912.

DOI: 10.1021/acsphotonics.6b00184
ACS Photonics 2016, 3, 904−911

(22) Liu, N.; Wen, F. F.; Zhao, Y.; Wang, Y. M.; Nordlander, P.; Halas, N. J.; Alu, A. Individual Nanoantennas Loaded with Three-Dimensional Optical Nanocircuits. *Nano Lett.* **2013**, *13*, 142−147.
(23) Large, N.; Abb, M.; Aizpurua, J.; Muskens, O. L. Photoconductively Loaded Plasmonic Nanoantenna as Building Block for Ultracompact Optical Switches. *Nano Lett.* **2010**, *10*, 1741−1746.
(24) Lee, J.-H.; You, M.-H.; Kim, G.-H.; Nam, J.-M. Plasmonic Nanosnowmen with a Conductive Junction as Highly Tunable Nanoantenna Structures and Sensitive, Quantitative and Multiplexable Surface-Enhanced Raman Scattering Probes. *Nano Lett.* **2014**, *14*, 6217−6225.
(25) Bohren, C. F.; Huffman, D. R. *Absorption and Scattering of Light by Small Particles*; Wiley-VCH: New York, NY, 1983.
(26) Knight, M. W.; King, N. S.; Liu, L.; Everitt, H. O.; Nordlander, P.; Halas, N. J. Aluminum for Plasmonics. *ACS Nano* **2014**, *8*, 834−840.
(27) Naik, G. V.; Liu, J.; Kildishev, A. V.; Shalaev, V. M.; Boltasseva, A. Demonstration of Al: ZnO as a plasmonic component for near-infrared metamaterials. *Proc. Natl. Acad. Sci. U. S. A.* **2012**, *109*, 8834−8838.
(28) Boltasseva, A.; Atwater, H. A. Low-loss plasmonic metamaterials. *Science* **2011**, *331*, 290.
(29) Perez-Gonzalez, O.; Zabala, N.; Borisov, A. G.; Halas, N. J.; Nordlander, P.; Aizpurua, J. Optical Spectroscopy of Conductive Junctions in Plasmonic Cavities. *Nano Lett.* **2010**, *10*, 3090−3095.
(30) Scholl, J. A.; García-Etxarri, A.; Koh, A. L.; Dionne, J. A. Observation of Quantum Tunneling between Two Plasmonic Nanoparticles. *Nano Lett.* **2013**, *13*, 564−569.
(31) Fontana, J.; Ratna, B. R. Highly tunable gold nanorod dimer resonances mediated through conductive junctions. *Appl. Phys. Lett.* **2014**, *105*, 011107.
(32) Herrmann, L. O.; Valev, V. K.; Tserkezis, C.; Barnard, J. S.; Kasera, S.; Scherman, O. A.; Aizpurua, J.; Baumberg, J. J. Threading plasmonic nanoparticle strings with light. *Nat. Commun.* **2014**, *5*, 4568-1.
(33) González-Rubio, G.; González-Izquierdo, J.; Bañares, L.; Tardajos, G.; Rivera, A.; Altantzis, T.; Bals, S.; Peña-Rodríguez, O.; Guerrero-Martínez, A.; Liz-Marzán, L. M. Femtosecond Laser-Controlled Tip-to-Tip Assembly and Welding of Gold Nanorods. *Nano Lett.* **2015**, *15*, 8282−8288.
(34) Park, H. S.; Agarwal, A.; Kotov, N. A.; Lavrentovich, O. D. Controllable Side-by-Side and End-to-End Assembly of Au Nanorods by Lyotropic Chromonic Materials. *Langmuir* **2008**, *24*, 13833−13837.
(35) Adams, S. J. *Electromagnetic Theory*; McGraw Hill: New York, London, 1941.
(36) Nikoobakht, B.; El-Sayed, M. A. Preparation and growth mechanism of gold nanorods (NRs) using seed-mediated growth method. *Chem. Mater.* **2003**, *15*, 1957−1962.
(37) Fontana, J. P. Self-assembly and characterization of anisotropic metamaterials. Kent State University, 2011.
(38) Rakić, A. D.; Djurišić, A. B.; Elazar, J. M.; Majewski, M. L. Optical properties of metallic films for vertical-cavity optoelectronic devices. *Appl. Opt.* **1998**, *37*, 5271−5283.

DOI: 10.1021/acsphotonics.6b00184
ACS Photonics 2016, 3, 904−911